THERMODYNAMIC MODEL OF CRITICAL ICE-MELTING CURRENT ON ICED TRANSMISSION LINES

Yong-can ZHU[1], Xin-bo HUANG[*1], Long ZHAO[2], Yi TIAN[1], Jing-yu MU[3], Hua GAO[1]

[*1]College of Electronics and Information, Xi'an Polytechnic University, Xi'an, P.R.China 710048

[2]College of Electro-Mechanical Engineering, Xidian University, Xi'an, P.R.China 710071

[3]State Grid Anhui electric power company maintenance company, Hefei, P.R.China 230061

[*]Corresponding author; E-mail: huangxb1975@163.com

The thermal de-icing by Joule effect is a mostly valid way to prevent transmission lines from the severe ice storm. A model was put forward to simulate the critical ice-melting current on iced conductor. Based on this model, the value of critical ice-melting current was calculated with various parameters, some of which were ignored in the earlier literatures, such as ice-layer heat conductivity, wind attack angle, and icing section shape. The results of the experiment and simulation show that the critical ice-melting current increase with wind speed, wind attack angle, and ice-layer heat conductivity, but decrease rapidly with ambient temperature and LWC. Moreover, the maximum difference between the results of simulation and experiment is about 9%, thus this model can be employed to estimate the engineering parameters in practical thermal de-icing projects.

Key words: *transmission lines, icing, de-icing, critical ice-melting current*

1. Introduction

Transmission lines icing is one of the principal reasons of affecting the performance of the power system, which gives rise to a number of serious problems, such as flashover, structural failure, collapse of the tower, and even breakdown of the power grid [1-3]. In 1998, a severe ice storm took place in Eastern Canada and the Northeastern United States. Over 2,000,000 people lost power supply for weeks as 1,300 transmission towers and 35,000 distribution structures were damaged [4]. In 2008, at least 7,000 transmission lines above $10\,kV$ and 800 substations above $35\,kV$ were out of service, and more than 120,000 transmission towers were destroyed in China [5,6]. In order to solve the problem, academics and scientists dedicated into the research of transmission lines icing mainly by meteorology, fluid mechanics, and thermodynamics [4,7-8]. The thermal de-icing by Joule effect is a mostly valid way to prevent power grid from ice storms. Canada, China, and many other countries are all devoted to the study of thermal de-icing technology, and applied it on transmission lines [8-11]. However, in some heavy icing areas of China, the failure of de-icing project had happened because of inappropriate current density, so the accuracy of the ice-melting current has great theoretical significance and engineering value for the power enterprises [3].

The critical ice-melting current is the minimum current to trigger ice melting, which is the key parameter of the thermal de-icing project [3,12]. In 1980s, Personne carried out some meaningful

experiments to study the anti-icing current induced by the Joule effect for bare conductors, and gave a proposed estimation of the current to prevent the conductor from icing [13]. Makkonen proposed a model for icing accretion on transmission lines, and presented a significant heat balance equation for the iced conductor [4,14-15], which is often used in the models of icing growth and ice-melting. Jiang and Shu presented a heat balance model to calculate the critical ice-melting current of no-offset cylindrical glaze icing on transmission lines, and verified the calculation results by experiments in artificial climate chamber [3,16]. However, the research of critical ice-melting current ignored the complicated boundary conditions and the uneven temperature distribution of the icing shell, thus it is only valid for some typical conditions on iced transmission lines. In this paper, a model was proposed to simulate the critical ice-melting current. The local heat balance equations are used to analyze the temperature distribution of the iced conductor, and the complicated boundary conditions of heat transfer formulation are simplified in a proper way. Then, almost all the important influencing factors of heat balance equations are analyzed and validated.

2. Experimental method and apparatus

2.1. Experimental apparatus

As shown in Fig. 1(a), the artificial climate chamber is a closed rectangular ambience. The real experimental region of ice-melting is a rectangular duct of 1.5×0.8 m cross-section, which is separated by detachable plastic plates. Two test conductors are held horizontally with 0.8 m distance. With the refrigerator and electric heater, the temperature of the artificial climate chamber can be exactly controlled in -25 - +60 $°C$. The current circuit is supplied by a large current generator, four wall bushings, and two test conductors. The test current of the current circuit can rise to 2000 A.

In heavy icing areas of China, thousands of icing monitoring systems and observation stations are used to observe the phenomenon of icing growth. Literatures have established many mechanical calculation models for ice thickness and classified the iced conductors into circular shape, elliptical shape, sector shape, and wavy shape [11,17,18]. In this paper, a typical elliptical iced conductor is taken as an example to analyze the critical ice-melting, and its cross section is shown in Fig. 1(b).

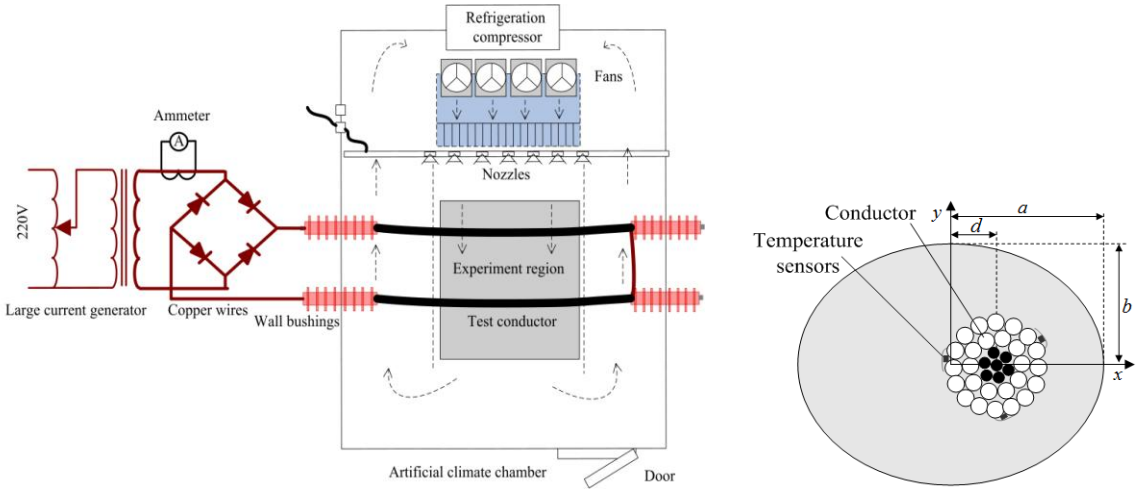

(a) The floor plan of artificial climate chamber (b) The schematic diagram of elliptical iced conductor

Fig. 1 The experimental apparatus

2.2. Experimental method of critical ice-melting current

As shown in Fig. 2, the physical properties of airstream are evaluated at ambient temperature (T_f) and wind speed (v), and the wind attack angle is expressed as θ. The conductor temperature (T_c) is measured by eight optical fiber temperature sensors which cling to the outside of the conductor. In order to determine the experimental value of critical ice-melting current as precisely as possible, 75 percent of the calculated value would be applied as the initial current, and it would be increased in a very small increment and a large time interval. The critical ice-melting current is defined as the experimental current when the first melting droplet is observed or the conductor temperature just equals to 0 $°C$.

3. Mathematical model

3.1. Heat transfer formulation

Before ice-layer melts, there is no air-gap and molten water. As shown in Fig. 2, the material region of iced conductor is divided into three parts: conductor (Θ_1), ice-layer (Θ_2), and airstream (Θ_3). The interfaces between adjacent regions are named conductor-ice (Γ_{12}) and ice-air (Γ_{23}), respectively. Moreover, the heat transfer equation in the Cartesian coordinate system is shown as

$$\rho_{\Theta k} c_{\Theta k} \frac{\partial T}{\partial \tau} - \frac{\partial}{\partial x}\left(\lambda_{\Theta k} \frac{\partial T}{\partial x} \right) - \frac{\partial}{\partial y}\left(\lambda_{\Theta k} \frac{\partial T}{\partial y} \right) - q_{\Theta k} = 0 \qquad k = 1,2,3 \tag{1}$$

where T denotes temperature, $°C$; $\rho_{\Theta k}$ denotes the mass density of region Θ_k, kg/m^3; $c_{\Theta k}$ denotes the specific heat of region Θ_k, $Jkg^{-1}°C^{-1}$; $\lambda_{\Theta k}$ denotes the thermal conductivity of region Θ_k, $Wm^{-1}°C^{-1}$; $q_{\Theta k}$ denotes the thermal source of region Θ_k, W/m^2, which can be expressed as

$$\begin{cases} q_{\Theta k} = I^2 r_{Tc} / A_{\Theta k} & k = 1 \\ q_{\Theta k} = 0 & k = 2,3 \end{cases} \tag{2}$$

where I is test current, A; r_{Tc} is conductor resistance at temperature T_c, Ω/m; $A_{\Theta k}$ is cross-sectional area of Θ_k, m^2.

3.2. Boundary conditions

3.2.1 Boundary condition of conductor-ice adjacent region

The experiment of critical ice-melting current is supposed to be the condition of steady heat conduction, so the Joule heat of critical ice-melting current is absolutely dissipated at the ice-air boundary. Moreover, the thermal conductivity of aluminum is up to 210 $Wm^{-1}°C^{-1}$, which is nearly 100 times of ice-layer. So it is a workable hypothesis that the conductor temperature radial distributing is uniform for the condition of critical ice melting, and the value is equal to 0 $°C$. The thermal source $q_{\Theta 1}$ is replaced by the first kind boundary condition at the interface Γ_{12}, which can be expressed as

$$T|_{\Gamma 12} = 0°C \tag{3}$$

3.2.2 Boundary condition of ice-air adjacent region

As shown in Fig. 2, the local heat equilibrium at interface Γ_{23} is dominated by many parameters, and most of them have been studied in literatures [4,19,20]. Nevertheless, the heat flux associated with supercooled water drops must be taken into account, because de-icing may be performed on such rainy days [20]. So the local heat equilibrium at interface Γ_{23} can be expressed as

$$q_{cd} = q_{cq} + q_e - q_{dp} - q_f \tag{4}$$

where q_{cd} denotes the local heat flux of conduction, W/m^2; q_{dp} denotes the local heat flux caused by supercooled water drops; q_{cq} denotes the local heat flux of convective heat transfer; q_e denotes the local heat flux of evaporation or sublimation. q_f denotes the impact of viscous heating by airstream; the effect of q_f is often ignored because it is much smaller.

With different accretion efficiency, the process of ice accretion is grouped into two categories: dry-growth and wet-growth. The analysis models and the critical condition of icing wet-growth to dry-growth have been introduced in literatures [4,19,21]. So in this paper, the ice-air interface can be divided into two parts, named $\Gamma_{23,w}$ and $\Gamma_{23,d}$. $\Gamma_{23,d}$ denotes the interface with icing dry-growth or no drops collision; $\Gamma_{23,w}$ denotes the drops collision region with icing wet-growth. Furthermore, there is a thin liquid layer on interface $\Gamma_{23,w}$, and the local temperature is equal to 0 $°C$ [4,21]. So it follows the first kind boundary condition, which can be expressed as

$$T|_{\Gamma 23,w} = 0°C \tag{5}$$

3.2.3 Boundary condition of $\Gamma_{23,d}$

For the interface $\Gamma_{23,d}$, the heat flux dependent surface temperature would be prescribed in the third kind boundary condition, and the rest heat flux would be applied on the thin ice-layer Θ_{23} (2~5 layer grid, clings to interface $\Gamma_{23,d}$) in the form of local equivalent thermal source, which can be respectively expressed as

$$\begin{cases} \lambda \dfrac{\partial T}{\partial n}|_{\Gamma 23,d} = h_{eq}(T_w - T_f) \\ q_{\Theta 23}|_{\Gamma 23,d} = \dfrac{C_{eq}}{A_{\Theta 23}} \end{cases} \tag{6}$$

where $\lambda \dfrac{\partial T}{\partial n}|_{\Gamma 23,d}$ denotes the heat flux of interface $\Gamma_{23,d}$ on the normal direction, W/m^2; T_w is local temperature of ice surface, $°C$; h_{eq} is the local equivalent coefficient of convective heat transfer, $Wm^{-2}°C^{-1}$; C_{eq} denotes the equivalent value of the local heat, W; $A_{\Theta 23}$ is the local area of Θ_{23}, m^2.

A. The heat flux caused by convective heat transfer

The heat flux of convective heat transfer is the major reason of heat dissipation, which can be expressed as

$$q_{cq} = h_{cq}(T_w - T_f) \tag{7}$$

where h_{cq} denotes the local convective heat transfer coefficient, $Wm^{-2}°C^{-1}$. In order to further reveal the effective law of h_{cq}, the finite element model and the SST (Shear Stress Transport) turbulence model can be used to improve the calculation accuracy [12,22,23].

B. The heat flux caused by sublimation

The natural air flow results in the increase of local sublimation heat flux q_e, which is usually calculated by the mass transfer coefficient. Furthermore, the heat flux of local sublimation can be described as [4,15,19]

$$q_e = \frac{\varepsilon L_v h_{cq}(e_w - e_f)}{C_{\Theta 3} P_{\Theta 3}} \tag{8}$$

where ε denotes the ratio of the molecular weights for water vapour and dry air; L_v is the specific latent heat of sublimation, J/kg; $P_{\Theta 3}$ is the static air pressure, P_a; e_w and e_f are the saturation water vapour pressures over the surface at T_w and T_f. The value of saturation water vapour pressure can be calculated by the Goff-Gratch formula which is officially recommended, but the computing process is much more complex. Considering that the surface temperature range of ice-melting is basically between -10 $°C$ and 0 $°C$, the approximate solution of saturation water vapour pressure with a linear equation is described as

$$e_t \approx 34.8T + 589 \qquad -10°C < T < 0°C \tag{9}$$

Substituting Eq. (9) in Eq. (8), the local heat flux of sublimation can be expressed as

$$q_e = h_e(T_w - T_f) \tag{10}$$

where h_e is equivalent local convective heat transfer coefficient for sublimation, it can be described as

$$h_e = \frac{34.8\varepsilon L_v h_{cq}}{C_{\Theta 3} P_{\Theta 3}} \tag{11}$$

C. The heat flux caused by supercooled water drops

The local heat flux, caused by supercooled water drops (q_{dp}), is mainly determined by four parameters. The heat flux released by cooling frozen droplets (q_{iw}), the heat flux associated with the release of latent heat (q_{ic}), the heat flux required to heat impinging precipitation (q_{mw}), and the heat flux absorbed from the kinetic energy of droplets (q_v). It can be described as

$$q_{dp} = q_{mw} + q_{ic} + q_{iw} + q_v \tag{12}$$

The terms in Eq. (12) can be expressed respectively, as

$$\begin{cases} q_{mw} = m_{im} c_w (T_f - T_0) \\ q_{ic} = m_{im} L_{ice} \\ q_{iw} = m_{im} c_{ice} (T_0 - T_w) \\ q_v = 0.5 m_{im} v^2 \end{cases} \tag{13}$$

where c_w and c_{ice} are the specific heat of water and ice, respectively, $Jkg^{-1}{}^{\circ}C^{-1}$. T_0 denotes the freezing temperature; L_{ice} denotes the latent heat of ice-freezing, J/kg; m_{im} is the mass of local icing accretion, $kgm^{-2}s^{-1}$. The local heat flux q_{dp} also can be expressed as the third kind boundary condition and equivalent thermal source

$$q_{dp} = h_{dp}(T_w - T_f) + \frac{C_{dp}}{A_{\Theta 23}} \tag{14}$$

where h_{dp} and C_{dp} are equivalent local convective heat transfer coefficient and equivalent local thermal source for the effect of supercooled water drops. They can be expressed as

$$\begin{cases} h_{dp} = -m_{im} c_{ice} \\ C_{dp} = m_{im} c_w (T_f - T_0) + m_{im} c_{ice} (T_0 - T_f) + m_{im} L_{ice} + 0.5 m_{im} v^2 \end{cases} \tag{15}$$

m_{im} is the key factor of q_{dp}, which can be expressed by Makkonen Model of icing growth [4,19]. In conclusion, the parameters of C_{eq} and h_{eq} in Eq. (6) can be expressed as

$$\begin{cases} h_{eq} = h_{cq} + \dfrac{34.8\varepsilon L_v h_{cq}}{C_{\Theta 3} P_{\Theta 3}} - m_{im} c_{ice} \\ C_{eq} = m_{im} c_w (T_f - T_0) + m_{im} c_{ice} (T_0 - T_f) + m_{im} L_{ice} + 0.5 m_{im} v^2 \end{cases} \tag{16}$$

3.3. Numerical Solution Method

The fluid-solid coupling heat transfer of the iced-conductor can be solved with high accuracy by special software (like Matlab and ANSYS). As shown in Fig.3, the grid of the flow field is also divided into four regions, which is completely in conformity with Fig.2. It is assumed that the whole flow field is a circular structure with a radius of $0.4\,m$, and the mesh elements number for conductor, ice-layer, thin ice-layer, and airstream field is 9600, 12800, 50×32, 25600, respectively.

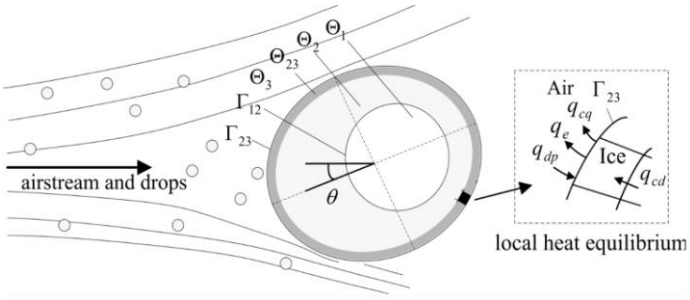

Fig. 2 The schematic diagram of heat transfer model

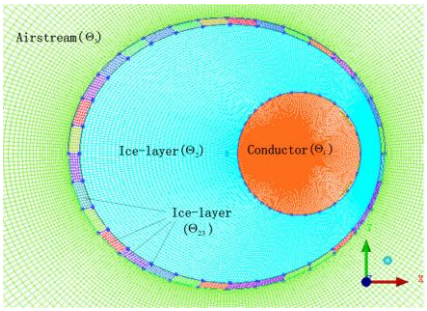

Fig. 3 The grid of iced conductor

In this paper, the local equivalent coefficient of convective heat transfer (h_{eq}), local thermal source (C_{eq}) and other boundary conditions will be calculated by combining of Fluent and Matlab. The main steps of this numerical simulation are listed as follows:

① The icing growth pattern will be analyzed on the given conditions, and the boundary condition of Γ_{23} can be classified.

② The mass of local icing accretion (m_{im}) must be calculated first with the airstream speed v.

③ The local convective heat transfer coefficient (h_{cq}) is calculated when the airstream speed is equal to v, then the value of h_{eq} and C_{eq} can be calculated by Eq.16.

④ The corrected airstream speed (v') will be analyzed according to the value of h_{eq}, and the convergence condition is defined as 1% difference between $\bar{h}_{cq}$ and $\bar{h}_{eq}$, where $\bar{h}_{cq}$ denotes the true average convective heat transfer coefficient for the corrected airstream speed v', and $\bar{h}_{eq}$ denotes the equivalent average coefficient of convective heat transfer for the true airstream speed v.

⑤ The critical ice-melting current will be calculated by the special software Fluent with the modified input parameters of v', T_f, C_{eq} and other boundary conditions. In addition, the residual monitors of energy, speed, and turbulence model parameters are set as 1×10^{-11}, 1×10^{-6}, and 1×10^{-6}, respectively. Based on this, the numerical simulation model of critical ice-melting current can quickly converge with the iteration number of 600-1000.

4. Simulation results

4.1. Effect of the wind attack angle

As a case in point, the cross-sectional shape of elliptical iced conductor is shown in Fig. 1(b). The

semi-major axis a, semi-minor axis b, and offset distance d are set as 17.5 mm, 15 mm, and 8 mm, respectively. The conductor radius is equal to 6.8 mm, and the resistance is about 0.31 Ω/km. The ambient temperature and wind speed is controlled in -5 $°C$ and 5 m/s. Moreover, the icing type is glaze with thermal conductivity equal to 2.2 $Wm^{-1}°C^{-1}$.

The simulated temperature distribution maps of ice-layer with different wind attack angles are shown in Fig. 4. When wind attack angle is 0°, the maximum value of local convective heat transfer coefficient locates at the front stagnation point (FSP). Moreover, the area of FSP is far away from the thermal source, so its local temperature is as low as -3.0 $°C$ in Fig 4(a). By contrast, the highest surface temperature locates at back stagnation point, and the value is about -0.5 $°C$. When wind attack angle is 180° (Fig. 4(c)), the highest local surface temperature situates at the front stagnation point with the value of -0.7 $°C$, and the lowest temperature lies at back stagnation point with -2.3 $°C$. Fig. 4(b) illustrates the temperature distribution map for the condition of 90° wind attack angle, and the range of surface temperature is between -2.4 $°C$ and -0.2 $°C$.

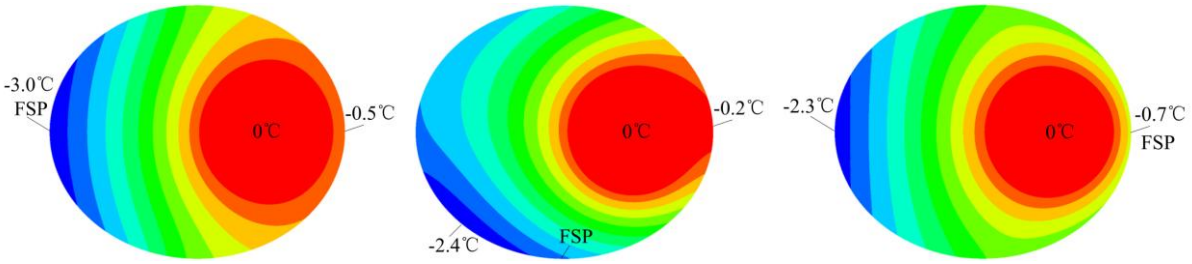

(a) θ=0° (b) θ=90° (c) θ=180°

Fig. 4 The temperature distribution maps of ice-layer with wind attack angle

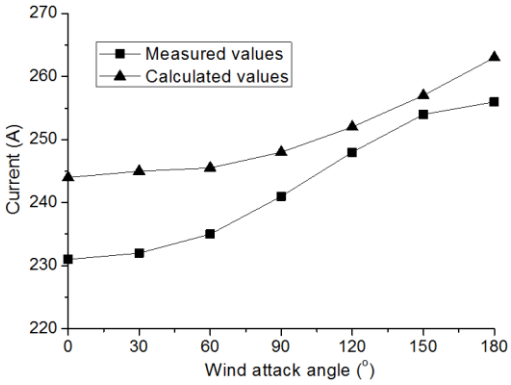

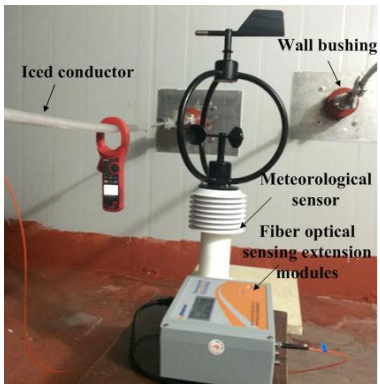

(a) The curve of critical ice-melting current (b) Experimental photograph

Fig. 5 The curve of critical ice-melting current versus wind attack angle

Influenced by the local temperature and convective heat transfer coefficient, the critical ice-melting current is variable with wind attack angles. As shown in Fig. 5(a), the calculated value of critical ice-melting current almost has no change when wind attack angle is less than 60°, approximately equal to 245 A. However, it gradually increases when wind attack angle is between 60° and 180°, and the maximum value is about 263 A, which has 8 percent increment compared to the condition of θ=0°. It is a good approach to slightly increase current density in the practical ice-melting projects, because of wind direction change and iced conductor rotation. The maximum relative difference between the experimental result and prediction is about 5%, and the results of experiment are always lower than numerical calculation values for all wind attack angles. This phenomenon should be explained by two reasons. On the one hand, the test data are obtained by the small-scale

experiments, so the external heat energy will flux into the test sample through the four wall bushings. On the other hand, the density of icing sample is generally between 800 kg/m^3 and 880 kg/m^3, so the actual thermal conductivity of ice-layer is slightly less than the simulation parameter.

4.2. Effect of meteorological parameters

Environmental wind speed is an important factor for icing growth and ice-melting. Keeping the model conditions depicted in Section 4.1, the critical ice-melting current versus wind speed is presented in Fig. 6. Because the surface heat dissipation caused by convective heat transfer and evaporation significant increases with wind speed, the critical ice-melting current increases with wind speed as well. When the wind speed is lower than 7.5 m/s, the critical ice-melting current is approximately proportional to the wind attack angle. Moreover, the calculated results (C) are in coincidence with experimental measurement (M) generally.

Similar to the effect of wind speed, ambient temperature is another significant influencing factor of heat balance. The surface dissipated heat is linearly associated with temperature difference between airstream and ice surface. So it is obvious that, the lower the ambient temperature is, the more heat it is required to trigger ice-melting. As shown in Fig. 7, the calculated ice-melting current increases with wind attack angle, but decreases quickly with ambient temperature. In addition, the maximum difference between experimental result and prediction is not significant, about 5.6%.

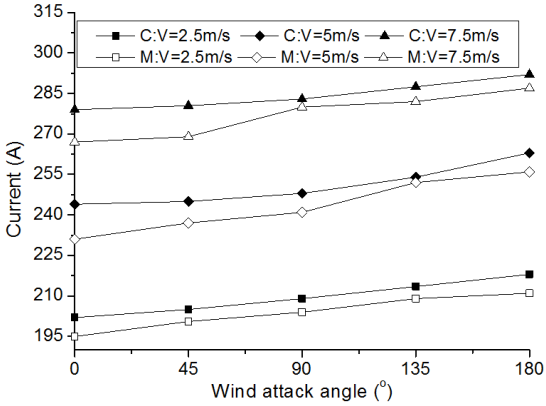

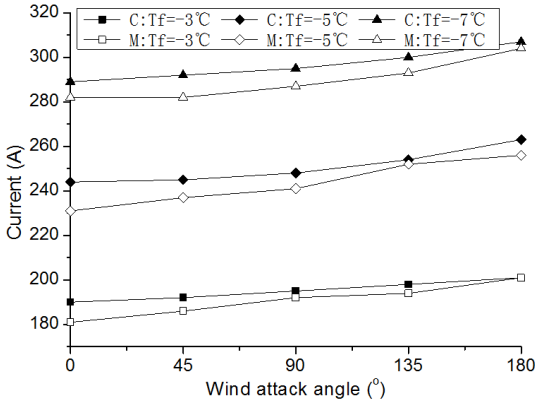

Fig. 6 The curve of critical ice-melting current versus wind speed

Fig. 7 The curve of critical ice-melting current versus ambient temperature

4.3. Effect of icing cross-sectional shape

It is difficult for us to define the cross-section shape of iced conductor exactly, but the approximate circular shape or elliptical shape is more common in excessive icing-disasters [11]. Keeping icing total mass as constant, the semi-minor axis of elliptical iced conductor is respectively set in 16.2 (circular), 16, 15.5, 15, 14.5, and 14 mm. The curves of critical ice-melting current with different semi-minor axis are shown in Fig. 8. It is observed that the critical ice-melting current is slightly influenced by the cross-section shape, and the maximum difference is only 7 A. When wind attack angle is 90°, the critical ice-melting current with different cross-section shape is nearly identical, and the value is about 247 A. In addition, the difference of critical ice-melting current is quite a little for various cross-section shapes, which is smaller than the error between the simulation and experimental result. So there is no sense in performing the experiment for different cross-section shapes.

When the offset distance is between 0 mm and 8 mm, the curve of critical ice-melting current versus wind attack angle is shown in Fig. 9. Compared with the effect of cross-sectional shape, the parameter of offset distance may have more influence. When offset distance is 0 mm, the value of critical ice-melting current hardly changes. But on the condition of $d>0mm$, the growth rate of critical ice-melting current increases with the offset distance. Compared with the condition of $d=0mm$, the critical ice-melting current for $d=8mm$ reduces 3 percent when wind attack angle is 0°, but the increment is more than 6 percent when wind attack angle is 180°.

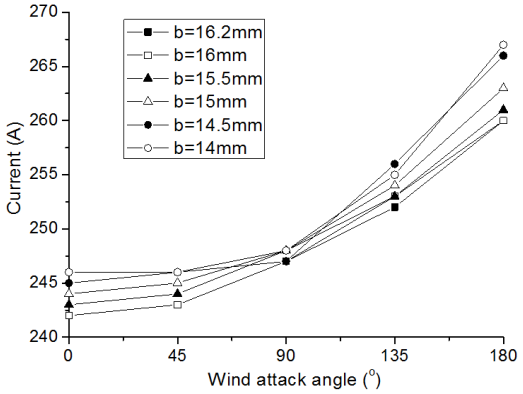

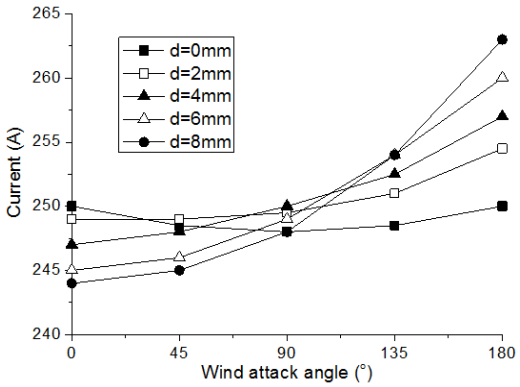

Fig. 8 The curve of critical ice-melting current versus icing shape

Fig. 9 The curve of critical ice-melting current versus offset distance

4.4. Effect of ice-layer thermal conductivity

The ice-layer thermal conductivity increases following density. Fukusako, Sturm, and Zhu respectively presented the quadratic equation in thermal conductivity and density, and found that the thermal conductivity of snow and soft rime is much less than 1.0 $Wm^{-1}°C^{-1}$ [24-26]. Unfortunately, due to the limitations of the experimental approach mentioned above, it is difficult to accurately adjust the test parameters of icing thermal conductivity in artificial icing laboratory. So this paper is just simulative study on the effect of icing thermal conductivity. Keeping the parameters shown in Section 4.1, the icing thermal conductivity is set as 0.5, 1.0, and 2.2 $Wm^{-1}°C^{-1}$, respectively. The calculated value of critical ice-melting current is shown in Fig. 10. Higher icing thermal conductivity results in higher surface temperature and more dissipation heat, so the critical ice-melting current increases rapidly with icing thermal conductivity. Compared with the condition of $\lambda_{\Theta 2}=0.5Wm^{-1}°C^{-1}$, the increment current is about 60 A for the glaze icing sample with $\lambda_{\Theta 2}=2.2Wm^{-1}°C^{-1}$. Therefore, it is essential for power companies to change the current density in practical de-icing engineering for different icing types.

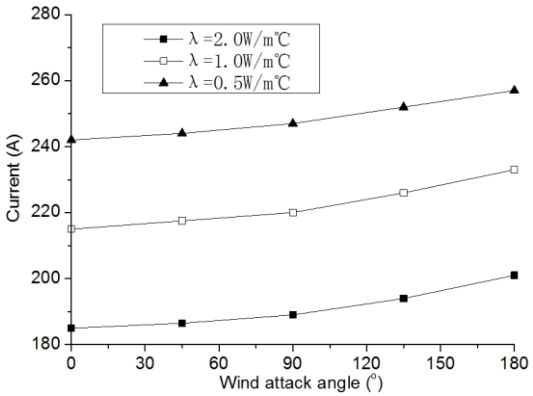

Fig. 10 The curve of critical ice-melting current versus ice-layer heat conductivity

4.5. Effect of supercooled water drops

The thermal de-icing by Joule effect tends to occur on rainy days, so the heat balance model is closer to the real ice-melting condition when supercooled water drop is introduced. When the Cartesian coordinate system is built with the origin at the front stagnation point and the medium volume diameter equal to 29 μm, the maximum value of local collision coefficient locates at the front stagnation point, and drops down quickly along the ice surface. On the condition of $\theta = 0°$, the maximum local collision efficiency is up to 0.48. When the wind attack angle is equal to 45° and 90°, the local collision coefficient at the front stagnation point decreases obviously, but the average value is slightly increases.

The released latent heat during drops freezing transports from the ice-air interface into ice-layer and airstream, and the temperature distribution of iced conductor increases as well. On the condition of $\mathrm{LWC} = 0.6g/m^3$ and $\theta = 0°$ (Fig. 11(a)), the lowest local temperature is about -1.5 $°C$, and the highest surface temperature locates at back stagnation point, with the value of -0.5 $°C$. When wind attack angle is 180°, it can be seen from Fig. 11(c) that the highest local surface temperature situates at the front stagnation point with the value of -0.02 $°C$, and the lowest temperature lies at back stagnation point with -2.3 $°C$. Fig. 11(b) illustrates the temperature distribution map when wind attack angle is equal to 90°, and the range of surface temperature is between -1.7 $°C$ and -0.1 $°C$.

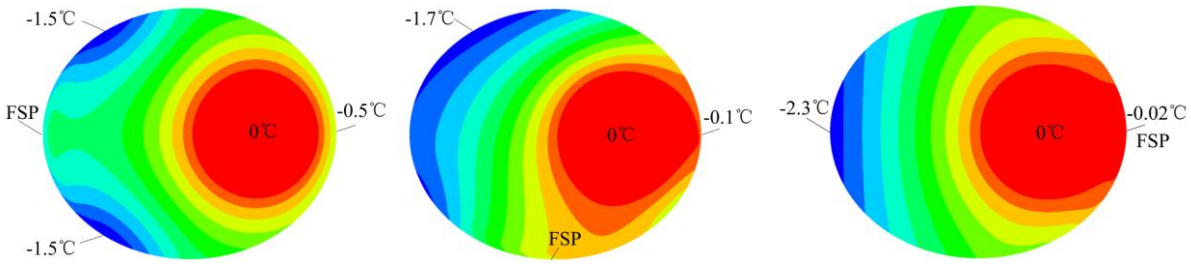

(a) θ=0° (b) θ=90° (c) θ=180°

Fig. 11 The temperature distribution maps of ice-layer when $LWC = 0.6g/m^3$

The curve of critical ice-melting current versus LWC is illustrated in Fig. 12. On the condition of $\mathrm{LWC} = 0.4g/m^3$, the temperature of icing surface is lower than 0 $°C$, then the icing growth belongs to dry-growth. The variation of critical ice-melting current with wind attack angle is very small, and the maximum relative difference is about 3 percent. On the condition of $\mathrm{LWC} = 0.8g/m^3$, more freezing latent heat is released on the upwind side of the iced conductor. The local icing growth type changes into wet-growth, and the value of critical ice-melting current decreases obviously. Moreover, the critical ice-melting current gradually decreases with wind attack angle, which just opposites to the above cases. In addition, the maximum relative difference between experiment and prediction exceeds 9 percent. The significant increment of relative difference may be caused by two reasons. Firstly, the unfrozen surface liquid would be frozen in other areas with more latent heat released. Secondly, the temperature of supercooled water is not as low as airstream, so the true heat flux of heat impinging precipitation is less than the calculated value.

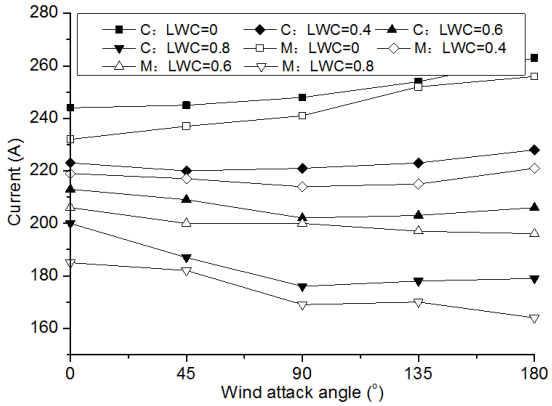

Fig. 12 The curve of critical ice-melting current versus LWC

5. Conclusion

1) A thermodynamic model is presented to simulate the critical ice-melting current of thermal de-icing by Joule effect, and the maximum relative error is about 9%.

2) The critical ice-melting current is almost identical when wind attack angle is less than 60°, but it gradually increases when wind attack angle is between 60° and 180°. In general, the maximum effect of wind attack angle on the critical ice-melting current is about 10%.

3) The parameter of supercooled water drops must be considered in critical ice-melting current model, because a massive source of heat will be released in the process of drops freezing.

4) The parameter of thermal conductivity has a significant impact on heat conduction and temperature distribution. It is essential for power companies to change the current density for different icing types in practical de-icing engineering.

Acknowledgements

This work is supported by the National Natural Science Foundation of China (Grant No. 51177115) and the Project of Doctoral Research Foundation of Xi'an Polytechnic University (Grant No. BS1703).

References

[1] Makkonen, L., Modeling power line icing in freezing precipitation, *Atmospheric research, 46* (1998), 1, pp. 131-142

[2] Péter, Z., *et al*., Numerical investigations of a new thermal de-icing method for overhead conductors based on high current impulses, *IET Generation, Transmission & Distribution, 2*(2008), 5, pp. 666-675

[3] Jiang, X., et al., Analysis of Critical Ice-melting Current for Short-circuit DC Transmission Line, *Proceedings of the CSEE, 30* (2010), 1, pp. 2032-2037 (in Chinese)

[4] Farzaneh, M., *Atmospheric icing of power networks*, Springer Science & Business Media., Berlin, Germany, 2008

[5] Xu, S., et al., Review of ice storm cases impacted seriously on power systems and de-icing technology, *Southern Power System Technology, 2* (2008), 2, pp. 1–6 (in Chinese)

[6] Hu Y., Analysis and Countermeasures Discussion for Large Area Icing Accident on Power Grid, *High Voltage Engineering*, *34*(2008), 2, pp. 215-219 (in Chinese)

[7] Druez, J., et al., Ice shedding from cables, *Cold regions science and technology, 23*(1995), 4, pp. 377-388

[8] Sadov, S. Y., et al., Mathematical model of ice melting on transmission lines, *Journal of Mathematical Modelling and Algorithms, 6*(2007), 2, pp. 273-286

[9] Alexandrov, B., et al., Preventing icing on Bashkir power grid, *Electric Safety Technology, 1*(1999), 1, pp. 14–16

[10] Dery. A., et al., Hydro-Quebec de-icing project, *Proceedings,* 11# Workshop on Atmospheric Icing of Structures Conf., Montreal, Canada, 2005

[11] Fan, S., et al., DC ice-melting model for elliptic glaze iced conductor, *IEEE Transactions on Power Delivery, 26*(2011), 4, pp. 2697-2704

[12] Péter, Z., Modeling and simulation of the ice-melting process on acurrent-carrying conductor, *UNIVERSITÉ DU QUÉBEC*, doctorate QUEBEC, 2006

[13] Personne, P., et al., Ice accretion on wires and anti-icing induced by Joule effect, *Journal of Applied Meteorology, 27(1988)*, 2, pp. 101-114

[14] Makkonen, L., Estimating intensity of atmospheric ice accretion on stationary structures, *Journal of applied meteorology, 20* (1981), 5, pp. 595-600

[15] Makkonen, L., Modeling of ice accretion on wires, *Journal of Climate and Applied Meteorology, 23* (1984), 6, pp. 929-939

[16] Jiang, X., et al., Critical Ice-Melting Current of Ice-Covered OPGW and Its Impacting Factors, *Transactions of China Electrotechnical Society*,*31* (2016), 9, pp. 174-180 (in Chinese)

[17] Huang, X., et al., A new on-line monitoring technology of transmission line conductor icing, *IEEE International Conference on Condition Monitoring and Diagnosis*, Bali, Indonesia, 2012

[18] Jiang, X., et al., Predictive Model for Equivalent Ice Thickness Load on Overhead Transmission Lines Based on Measured Insulator String Deviations, *IEEE Transactions on Power Delivery, 29* (2014), 4, pp. 1659-1665

[19] Makkonen, L., Models for the growth of rime, glaze, icicles and wet snow on structures, *Philosophical Transactions of the Royal Society of London A: Mathematical, Physical and Engineering Sciences, 358* (2000), pp.2913-2939

[20] Huneault, M., Combined models for glaze ice accretion and de-icing of current-carrying electrical conductors, *IEEE Transactions on Power Delivery, 20*(2005), 2, pp.1611-1616

[21] Sun, C., et al., Analysis of critical icing conditions of conductor and wet-dry-growth. *Proceedings of the CSEE, 23* (2003), 3, pp.141-145 (in Chinese)

[22] Menter, F. R., et al., Ten years of industrial experience with the SST turbulence model, *Turbulence, heat and mass transfer, 4* (2003), 1, pp. 625-632

[23] Mostafa, M. S., et al. Flow and heat transfer characteristics around an elliptic cylinder placed in front of a curved plate[J]. *Thermal Science*, 18(2014), 2, pp.465-478

[24] Fukusako, S., Thermophysical properties of ice, snow, and sea ice, *International Journal of Thermophysics, 11*(1990), 2, pp. 353-372

[25] Zhu, Y., et al., Experimental study on the thermal conductivity for transmission line icing. *Cold Regions Science and Technology, 129*(2016), 9, pp. 96-103

[26] Sturm, M., et al., The thermal conductivity of seasonal snow, *Journal of Glaciology, 43*(1997), pp. 26-41